

A spiral variable section capillary model for piping hydraulic gradient of soils causing water/mud inrush in tunnels

P. Lin^{1a}, S.C. Li^{1b}, Z.H. Xu^{*1}, L.P. Li^{1c}, X. Huang^{1d}, S.J. He^{1e}, Z.W. Chen^{2f}
and J. Wang^{1g}

¹Geotechnical & Structural Engineering Research Center, Shandong University, Jinan, Shandong, 250061, China

²School of Mechanical and Mining Engineering, the University of Queensland, St. Lucia, QLD 4072, Australia

(Received October 14, 2016, Revised April 22, 2017, Accepted May 23, 2017)

Abstract. An innovative spiral variable-section capillary model is established for piping critical hydraulic gradient of cohesion-less soils causing water/mud inrush in tunnels. The relationship between the actual winding seepage channel and grain-size distribution, porosity, and permeability is established in the model. Soils are classified into coarse particles and fine particles according to the grain-size distribution. The piping critical hydraulic gradient is obtained by analyzing starting modes of fine particles and solving corresponding moment equilibrium equations. Gravities, drag forces, uplift forces and frictions are analyzed in moment equilibrium equations. The influence of drag force and uplift force on incipient motion is generally expounded based on the mechanical analysis. Two cases are studied with the innovative capillary model. The critical hydraulic gradient of each kind of sandy gravels with a bimodal grain-size-distribution is obtained in case one, and results have a good agreement with previous experimental observations. The relationships between the content of fine particles and the critical hydraulic gradient of seepage failure are analyzed in case two, and the changing tendency of the critical hydraulic gradient is accordant with results of experiments.

Keywords: capillary model; piping; cohesion-less soils; critical hydraulic gradient; incipient motion

1. Introduction

Large quantities of water-rich tunnels will be built with the great development of transport. Disasters often happen in water-rich tunnels such as water gushing, mud inrush, surrounding rock collapse and so on (Yuan *et al.* 2016, Li *et al.* 2016). These disasters are common caused by

*Corresponding author, Associate Professor, E-mail: zhenhao_xu@sdu.edu.cn

^aPh.D. Student, E-mail: sddxytlp@163.com

^bProfessor, E-mail: lishucais@sdu.edu.cn

^cProfessor, E-mail: yuliyangfan@163.com

^dPh.D. Student, E-mail: hx19891018@yeah.net

^eMaster Student, E-mail: hsj686@126.com

^fLecturer, E-mail: zhongwei.chen@uq.edu.au

^gLecturer, E-mail: wjingsdu@163.com

seepage failure in water-rich tunnels. Seepage failure (such as piping) easily occurs in porous soils or fracture rock mass because fine particles running away often induces instability of soil (Liu *et al.* 2013, Yang *et al.* 2015). Actually, piping has been a common disaster in dam and subgrade projects (Chen *et al.* 2012, Okeke *et al.* 2016, Serdar *et al.* 2015). In recent years, disasters induced by piping failure attracts attention in water-rich tunnels (Bai *et al.* 2013, Ma *et al.* 2016, Ni *et al.* 2010, Qin *et al.* 2013). Mechanism researches of piping failure are mostly focused on determining of seepage type and critical hydraulic gradient of piping failure (Alhasan *et al.* 2015, Chen *et al.* 2015, Duan *et al.* 2015, Indraratna *et al.* 2002, Richards *et al.* 2007). Seepage type is determined according to the content of fine particles. The distinction between fine particles and coarse particles is usually defined by grain-size distribution. The piping critical hydraulic gradient is mostly obtained by experiments (Moffat *et al.* 2011, Yang *et al.* 2016), but theoretical methods are not mature (Chang *et al.* 2013, Ojha *et al.* 2003). Capillary model is usually used to study seepage characteristics of porous medium because capillary model can conveniently and efficiently describe fine particles movement and analyze force and moment equilibriums. Pore space of porous medium is simplified to a series of parallel capillaries, and pore volume is equal to total capillary volume. Various capillary models are applied to study piping, such as straight capillary model, winding capillary model, same-diameter capillary model and variable-section capillary model. Same-diameter capillary model do not suit to describe non-laminar flow, but variable-section capillary model can make up the defect. Variable-section capillary model is widely used to calculate the piping critical hydraulic gradient (Indraratna *et al.* 2002, Liu *et al.* 2004). Straight capillary model ignores the actual winding seepage channel. Few researches about winding capillary model for piping are reported. The incipient motion of fine particles is solved usually based on force and moment equilibrium equations. Previous methods almost only analyze gravity and drag force (Indraratna *et al.* 2002, Liu 1992). However, uplift force also plays an important role in fine particles starting. In addition, straight capillary model cannot describe uplift force during piping in vertical direction.

An innovative spiral variable-section capillary model is proposed for piping critical hydraulic gradient of cohesion-less soils. Cohesion-less soils are divided into coarse particles and fine particles according to grain-size distribution in this model. Pore space of coarse particles is simplified to a series of spiral variable-section capillaries. The curvature is proposed to quantitatively describe the actual winding seepage channel. Relationships between curvature and particle gradation, porosity, permeability are established. Different force and moment equilibrium equations are established based on different fine particles starting modes. The critical hydraulic gradient and the incipient velocity are obtained by solved equilibrium equations. Two cases are studied with this model and results are in good agreement with previous achievements.

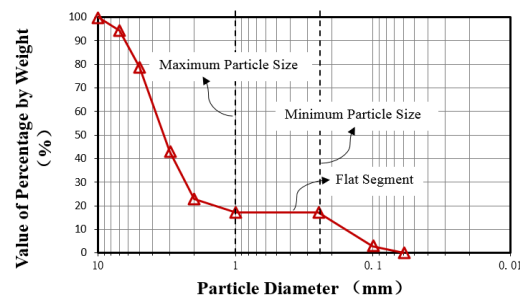


Fig. 1 Bimodal grain-size distribution curve

2. An innovative spiral variable-section capillary model

2.1 Determining of fine particles and porosity of hypothetical soil

Piping-typed soil particles are usually classified into coarse particles and fine particles (Aberg 1992, Liu *et al.* 2004). Coarse particles are fixed as the framework of soil. Fine particles can move in a certain space under high hydraulic gradient conditions. Fine particles and coarse particles are determined according to grain-size distribution.

There is at least one grade of particles whose content is less than or equal to 3% in bimodal grain-size-distribution soils. A corresponding flat segment exists in the grain-size distribution curve, as shown in Fig. 1. And the determining particle size (d_f) is defined by the average of the maximum and the minimum particle size or equal to the minimum particle size in the flat segment.

The determining particle size (d_f) in unimodal grain-size-distribution soils is defined by Eq. (1) (Liu 1992)

$$d_f = \sqrt{d_{70}d_{10}} \tag{1}$$

where d_{70} indicates one limit particle size, and the weight ratio of particles (whose size are less than d_{70}) is 70%; d_{10} indicates another limit particle size, and the weight ratio is 10%.

Porosity (φ) of hypothetical soil (composed of coarse particles) can be obtained by Eq. (2)

$$\varphi = \frac{e + S_{vf}}{1 + e} \tag{2}$$

where S_{vf} indicates the volume ratio of fine particles to all particles, e is porosity ratio of original soils.

2.2 Quantity and curvature of capillary

Pore space of hypothetical soil is simplified to a series of spiral capillaries as shown in Fig. 2. Mean diameter and curvature of each capillary are the same. Curvature indicates the ratio of capillary length (actual seepage channel) to soil length.

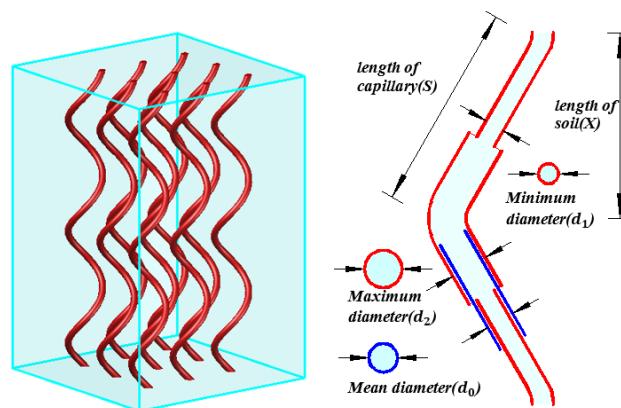


Fig. 2 Spiral variable-section capillary model for hypothetical soil

Water flow (Q_1) of all capillaries is calculated based on Poiseuille's formula as represented by Eq. (3) (Qin *et al.* 2004)

$$Q_1 = N \frac{\pi d_0^4 (P_1 - P_2)}{128 \mu S} \quad (3)$$

where N is the quantity of capillaries, d_0 is the mean diameter of each capillary, μ is water viscosity coefficient, S is the length of each capillary, $P_1 - P_2$ is water pressure difference.

Water flow (Q_2) of hypothetical soil is calculated based on Darcy's formula as represented by Eq. (4)

$$Q_2 = \frac{kA(P_1 - P_2)}{\mu X} \quad (4)$$

where k indicates the permeability of hypothetical soil, X indicates the length of soil, A indicates the cross-section area of soil.

Q_1 is equal to Q_2 , so Eq. (5) is obtained

$$N \frac{\pi d_0^4 (P_1 - P_2)}{128 \mu S} = \frac{kA(P_1 - P_2)}{\mu X} \quad (5)$$

The quantity of capillaries per unit area is calculated by Eq. (6) through solving Eq. (5)

$$n = \frac{128kT}{\pi d_0^4} \quad (6)$$

where n is the quantity of capillaries per unit area, $n=N/A$. T is curvature of each capillary, T is calculated by Eq. (7)

$$T = S/X \quad (7)$$

Pore volume of hypothetical soil is equal to all capillaries volume, so porosity can also be represented as Eq. (8)

$$\varphi = \frac{nA\pi d_0^2 S}{4AX} = \frac{nT\pi d_0^2}{4} \quad (8)$$

Curvature is obtained as represented by Eq. (9) through solving Eqs. (6) and (8)

$$T = \frac{d_0}{4\sqrt{2}} \cdot \sqrt{\varphi/k} \quad (9)$$

Curvature is affected by mean capillary diameter, porosity and permeability of hypothetical soil according to Eq. (8). In addition, mean capillary diameter is controlled by grain-size distribution of initial soil.

Helix angle of capillary is determined by curvature as shown in Eq. (10).

$$\theta = \arcsin(1/T) \quad (10)$$

2.3 Coefficient of variable-section capillary

Variable-section capillary usually has two diameters, as shown in Fig. 2. Kovacs obtains mean diameter, minimum diameter and maximum diameter of variable section capillary based on an assumption that the ratio of wall area to capillary volume is equal to the ratio of total particles' surface areas to soil pore volume (Liu *et al.* 2004).

Mean diameter (d_0) is defined by Eq. (11)

$$d_0 = \frac{2\phi D_h}{3(1-\phi)} \quad (11)$$

where D_h indicates effective particle diameter of hypothetical soil, as defined by Eq. (12)

$$D_h = \frac{1}{\sum \Delta S_i / D_i} \quad (12)$$

where ΔS_i indicates mass ratio of i th grade particles to total coarse particles, D_i is i th grade particle diameter.

Minimum diameter (d_1) is defined by Eq. (13) according to d_0

$$d_1 = d_0 / 1.5 \quad (13)$$

Maximum diameter (d_2) is defined by Eq. (14) also according to d_0

$$d_2 = 1.25d_0 \quad (14)$$

The length of large-section part of a capillary is equal to the length of small-section part, because capillary volume is unaltered. $l_1=l_2=l/2$, where l is the length of a total capillary, l_1 is the length of large-section part of the capillary, l_2 is the length of small-section part of the capillary.

3. Mechanism of incipient motion of fine particles

3.1 Forces acting on particles

Several main forces acting on particles are analysed: effective gravity, friction, drag force and uplift force.

Effective gravity is calculated from Eq. (15)

$$W' = 4/3 \pi d_s^3 (\rho_s - \rho) g \quad (15)$$

where ρ is fluid density, ρ_s is particle density, d_s is particle diameter.

Drag force is defined by Eq. (16)

$$F_D = C_D \frac{\rho v_0^2}{2} \frac{\pi d_s^2}{4} \quad (16)$$

where C_D is drag coefficient, v_0 is fluid velocity at the centre of a particle.

Drag coefficient is affected by Reynolds number (R_e). Many researches on drag coefficient is

conducted. Drag coefficient can be calculated by Eq. (17) (Stokes 1851).

$$C_D = \frac{24}{R_e} \tag{17}$$

where R_e is reproduced in Eq. (18).

$$R_e = \frac{d_s v_0 \rho}{\mu} \tag{18}$$

Uplift force is defined by Eq. (19)

$$F_L = C_L \frac{\rho v_0^2}{2} \frac{\pi d_s^2}{4} \tag{19}$$

where C_L is uplift coefficient.

A relationship between uplift coefficient and Reynolds number should be built similar to drag coefficient, yet relevant research achievements are rare. However, previous researches prove that values of drag force and uplift force belong to the same order of magnitude. In addition, some values of CD and CL are obtained by experiments, such as CD=0.47 and CL=0.1 by Eugeni Dementiev (Li *et al.* 1983), CD=0.78 and CL=0.18 by Han Qiwei (Han *et al.* 1999), CD=0.4 and CL=0.1 by Li Zhenru (Li *et al.* 1983). Thus, CL is equal to a quarter of CD in this article.

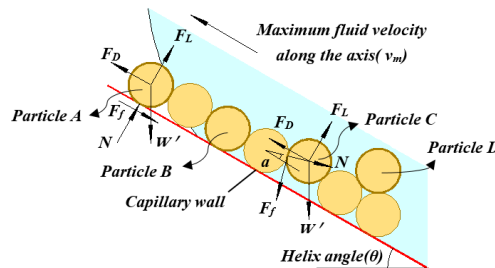


Fig. 3 Force analysis without particles interaction force

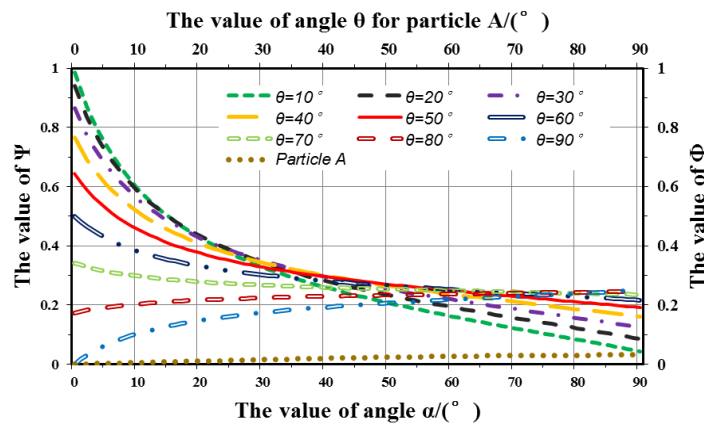


Fig. 4 Relation curves among $\Psi(\Phi)$, θ and α

3.2 Mechanical analysis and incipient velocity in capillary

There are four initial positions of movable particles in pore space, such as particle A, B, C and D, as shown in Fig. 3. Only drag force (F_D), uplift force (F_L), effective gravity (W'), friction (F_f) and normal force (N) are applied to mechanical analysis. Other forces are ignored so that the analysing process is simple. Only the moment equilibrium equation is used to define the incipient velocity because particles rotate more easily than slide. Particle A is subject to friction and normal force from capillary wall. So, particle A will rotate around contact point under the action of drag force, uplift force and effective gravity. In addition, particle A no longer touches the back particle. Discriminant function for incipient motion is defined by the Eq. (20) based on the above analysis

$$1/2W'd_s \sin \theta \leq 1/2F_D d_s \tag{20}$$

Eq. (20) is simplified to Eq. (21)

$$W' \sin \theta \leq F_D \tag{21}$$

The discriminant equation shows that only under the action of drag force can particle A start and migrate. The effect of uplift force is weak obviously.

Incipient velocity formula for particle A is obtained through substituting Eqs. (15) and (16) into Eq. (21) as shown in Eq. (22).

$$v_0 = \frac{16(\rho_s - \rho_w)gd_s^2 \sin \theta}{9\mu} \cdot \Phi \tag{22}$$

where Φ is represented by Eq. (23)

$$\Phi = \frac{\sin \theta}{32} \tag{23}$$

Particle C is subject to friction and normal force from the front particle, as shown in Fig. 3. So, particle C will rotate around contact point under the action of drag force, uplift force and effective gravity. In addition, particle C no longer touch the back particle. Discriminant function for incipient motion is defined by the Eq. (24)

$$1/2W'd_s \sin(\pi/2 + \theta - \alpha) \leq 1/2F_D d_s \sin \alpha + 1/2F_L d_s \cos \alpha (0 \leq \alpha \leq \pi/2) \tag{24}$$

Eq. (24) is simplified to Eq. (25)

$$W' \cos(\theta - \alpha) \leq F_D \sin \alpha + F_L \cos \alpha (0 \leq \alpha \leq \pi/2) \tag{25}$$

The effect of drag force disappears when α is zero, such as particle B. Only under the action of uplift force can Particle B escape from defenders. Uplift force plays a dominant role in particle starting at the position. The effect of uplift force disappears when α is $\pi/2$. The discriminant equation is the same as particle A.

Incipient velocity formula for particles B, C and D is obtained through substituting Eqs. (15), (16) and (19) into Eq. (25) as shown in Eq. (26).

$$v_0 = \frac{16(\rho_s - \rho_w)gd_s^2}{9\mu} \cdot \Psi \tag{26}$$

where Ψ is represented by Eq. (27)

$$\Psi = \frac{\cos(\theta - \alpha)}{(\cos \alpha + 4 \sin \alpha)} \tag{27}$$

Some researches on relations among Ψ (Φ), θ and α are conducted for analysing particles starting sequence as shown in Fig.4. Curve of Particle A shows the relation between Φ and θ . Curve of $\theta=10^\circ, \theta=20^\circ, \theta=30^\circ, \theta=40^\circ, \theta=50^\circ, \theta=60^\circ, \theta=70^\circ, \theta=80^\circ$ or $\theta=90^\circ$ shows the relation between Ψ and α .

When θ is $0^\circ, 10^\circ, 20^\circ, 30^\circ, 40^\circ, 50^\circ, 60^\circ$ and 70° , the value of Ψ decreases with angle α , and Ψ change slowly when θ is 70° ; but when θ is 80° and 90° , the value of Ψ increase with angle α . The value of Φ increase with angle θ according to Φ - θ relation curve for particle A. In addition, values of Φ are mostly less than values of Ψ . It indicates that particles starting sequence is: particle A>particle D>particle C >particle B.

4. Critical hydraulic gradient for incipient motion

Particles move in circular tube caused by fluid, as shown in Fig. 5. The maximum fluid velocity along the axis of capillary is reproduced in Eq. (28) according to Poiseuille's law.

$$v_m = v_0 \left(\frac{r^2}{r^2 - b^2} \right) \tag{28}$$

where v_m indicates maximum fluid velocity, v_0 is fluid velocity along the axis of particle, r is the radius of capillary, b is the distance from the particle centre to the axis.

Average velocity of cross section is defined by the maximum velocity as shown in Eq. (29).

$$v_a = v_m / 2 \tag{29}$$

where v_a indicates average fluid velocity of cross section.

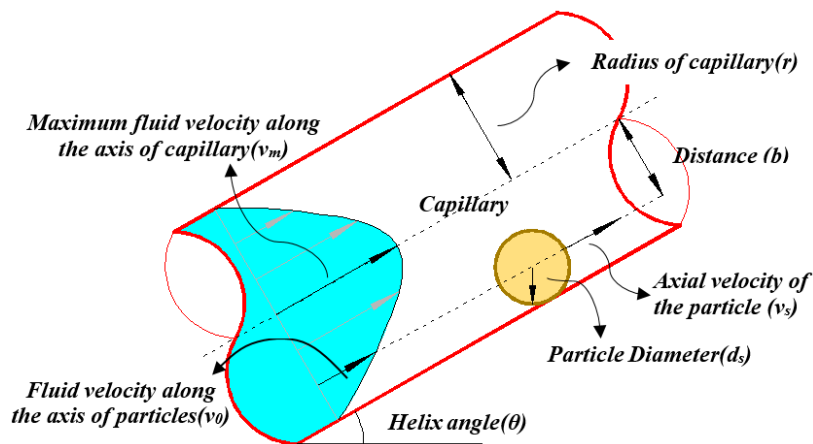


Fig. 5 Particle and fluid motion in a circular tube

Pressure drop caused by single particle in Poiseuille tube is calculated by Eq. (30) through Happel and Brenner's method (Liu 2001).

$$\Delta P_s = \frac{6\mu d_s}{r^2} \left(1 - \frac{b^2}{r^2}\right) \left[v_m \left(1 - \frac{b^2}{r^2}\right) - v_s \right] \quad (30)$$

where d_s is diameter of a particle, v_s is particle velocity.

v_s is zero when a particle is at rest or at the starting moment. So, Eq. (30) is simplified to Eq. (31).

$$\Delta P_s = \frac{6\mu d_s}{r^2} \left(1 - \frac{b^2}{r^2}\right) \left[v_m \left(1 - \frac{b^2}{r^2}\right) - v_s \right] \quad (31)$$

Pressure drop per unit length caused by friction of capillary wall is calculated by Eq. (32).

$$\Delta P_l = \frac{8\mu}{r^2} v_a T \quad (32)$$

Thus, total pressure drop in a single capillary is defined by Eq. (33).

$$\Delta P = \Delta P_l + \sum M_i \Delta P_s \quad (33)$$

where M_i indicates the quantity of i th grade particles. M_i is calculated by Eq. (34).

$$M_i = \frac{6s_{vi}}{n\pi d_{si}^3} \quad (34)$$

where n is the quantity of capillaries per unit area, s_{vi} indicates the volume ratio of i th grade fine particles to whole soil, s_{vi} is calculated by Eq. (35).

$$s_{vi} = S_{vi} (1 - \varphi) / (1 - S_{vf}) \quad (35)$$

where S_{vf} indicates the volume ratio of fine particles to all particles, S_{vi} indicates the volume ratio of i th grade particles to all particles, φ is porosity of hypothetical soils.

Thus, the critical hydraulic gradient for the incipient motion in a single capillary is obtained through Eq. (36).

$$i_{cr} = \frac{\Delta P}{\gamma_w T} \quad (36)$$

The hydraulic gradients relationship between large-section part and small-section part is defined by Eq. (37) when flow is constant.

$$Q = \frac{\gamma_w \pi d_1^4 i_1}{128\mu} = \frac{\gamma_w \pi d_2^4 i_2}{128\mu} \quad (37)$$

where i_1 is the hydraulic gradient in small-section part of capillary, i_2 is the hydraulic gradient in large-section part, d_2 is equal to $1.875d_1$ according to Eqs. (13) and (14).

Thus, the relationship is represented by Eq. (38).

$$i_1 = \left(\frac{d_2}{d_1} \right)^4 i_2 = 12.36i_2 \quad (38)$$

The hydraulic gradient in small-section part is 12.36 times larger than in large-section part. It means that particles in small-section part firstly start and migrate before particles in large-section part.

Particles content ratio is simplified to volume ratio in single capillary. So, particles quantity in small-section part is calculated by Eq. (39).

$$M_{1i} = M_i \frac{d_1^2}{d_1^2 + d_2^2} = 0.22M_i \quad (39)$$

And particles quantity in small-section part is calculated by Eq. (40).

$$M_{2i} = M_i \frac{d_2^2}{d_1^2 + d_2^2} = 0.78M_i \quad (40)$$

Total pressure drop caused by small-section part is determined by Eq. (41).

$$\Delta P_1 = 1/2\Delta P_{l1} + \sum M_{1i}\Delta P_{s1} \quad (41)$$

Total pressure drop caused by large-section part is determined by Eq. (42).

$$\Delta P_2 = 1/2\Delta P_{l2} + \sum M_{2i}\Delta P_{s2} \quad (42)$$

Water flow through soil is equal to flow through capillary model as shown in Eq. (43).

$$\frac{kA\gamma_w}{\mu} \cdot I_{cr} = N \frac{\pi d_1^4}{128\mu} \frac{\Delta P_1}{T/2} = N \frac{\pi d_2^4}{128\mu} \frac{\Delta P_2}{T/2} \quad (43)$$

Thus, the critical hydraulic gradient for incipient motion in soil is calculated by Eq. (44).

$$I_{cr} = \frac{n\pi d_1^4 \Delta P_1}{64k\gamma_w T} = \frac{n\pi d_2^4 \Delta P_2}{64k\gamma_w T} \quad (44)$$

And the incipient velocity in soil is calculated by Eq. (45)

$$I_{cr} = \frac{n\pi d_1^4 \Delta P_1}{64k\gamma_w T} = \frac{n\pi d_2^4 \Delta P_2}{64k\gamma_w T} \quad (45)$$

5. Examples and discussion

5.1 Case one

The proposed method is applied in a piping-typed sandy gravels with a bimodal grain-size-distribution. The sandy gravels are originally used for piping experiments by Skempton and J.M. Brogan. Grain-size distribution curve of sandy gravels is shown in Fig. 6 (Kempton *et al.* 1994).

Determining particle diameter (d_p) is 0.625 mm based on the grain-size distribution curve. Fine particles size includes 0.06 mm, 0.1 mm and 0.25 mm. The weight ratio of fine particles is 17.14%. Initial void ratio (e) is 0.471. Porosity (ϕ) of hypothetical soil is 0.437 according to Eq. (2). Effective particle diameter (D_h) is 3.17 mm according to Eq. (12). Mean capillary diameter (d_0) is 1.64 mm according to Eq. (13). The incipient velocity is calculated by Eq. (22) according to Particle A because about two fine particles are in per 10 mm-length capillary. Particles start freely without stumbling particles. Permeability of hypothetical soil is 4 cm/s according to previous study (Liu *et al.* 2004). Initial permeability is 0.45 cm/s. In addition, permeability is 0.9 cm/s when obvious piping happens.

Pressure drop caused by particles is so much less than pressure drop caused by capillary wall according to calculation as illustrated in Table 1. Thus, the formula of critical hydraulic gradient is simplified to Eq. (46)

$$I_{cr} = \frac{n\pi\mu d_1^2 v_{a1}}{4k\gamma_w} = \frac{n\pi\mu d_2^2 v_{a2}}{4k\gamma_w} \tag{46}$$

The critical hydraulic gradient is calculated by Eq. (46) and results are shown in Table 2.

Some conclusions are obtained from Table 1. Firstly, particles in small-section part of capillary start before particles in large-section part. Secondly, piping has four evolution process: Particles #1 (0.06 mm diameter) firstly start and migrate only in small-section part when hydraulic gradient

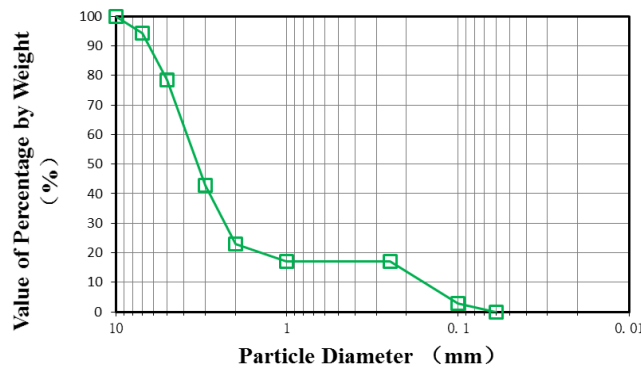


Fig. 6 Grain-size distribution curve of sand-gravel

Table 1 Pressure drop caused by particles and capillary wall

Particle diameter	Content	Quantity of particles	Pressure by capillary	Pressure by total particles
0.06 mm	2.9%	150	352 Pa	0.008 Pa
0.10 mm	14.3%	269	598 Pa	0.111 Pa

Table 2 The critical hydraulic gradient for incipient motion of fine particles

Particle diameter	Critical hydraulic gradient	
	in small-section part	in large-section part
0.06 mm	0.062	0.201
0.10 mm	0.105	0.339

reaches 0.062. Moving particles #1 may settle down through large-section part. Only few fine particles migrate in some position of soil. Then particles #2 (0.10 mm diameter) start and migrate only in small-section part when hydraulic gradient increases to 0.105. Gradually particles #1 also move in large-section part when hydraulic gradient reaches 0.201. Some particles migrate throughout whole soil at the moment. Finally, all fine particles start and migrate when hydraulic gradient reaches 0.339, and piping occurs obviously.

Results have a good agreement with experimental observations (Kempton *et al.* 1994): Few fine particles are dancing on the side of soil sample when hydraulic gradient is 0.10. Few fine particles begin to move upwards in several places on the top of sample when hydraulic gradient is 0.125; Gradually more particles migrate slightly in about twelve places when hydraulic gradient reaches 0.145; Large-scale particles migrate slightly and small tubular channels appear on sample side when hydraulic gradient is 0.17; Then tubular channels are everywhere when hydraulic gradient increases to 0.2; Finally, failure occurs obviously when hydraulic gradient reaches 0.28.

5.2 Case two

Many valuable researches about the relationship between fine particles content and hydraulic gradient of seepage failure have been done (Liu 1963, Liu 1992). A series of samples with a bimodal grain-size-distribution are applied according to sandy gravels in previous researches (Liu 1992). Fine particles content of these samples is 15% to 30%. Grain-size distribution curve of some samples are shown in Fig. 7. Determining particle size (d_f) is 0.9 mm. Fine particles diameter includes 0.2 mm, 0.4 mm, 0.65 mm and 0.8 mm.

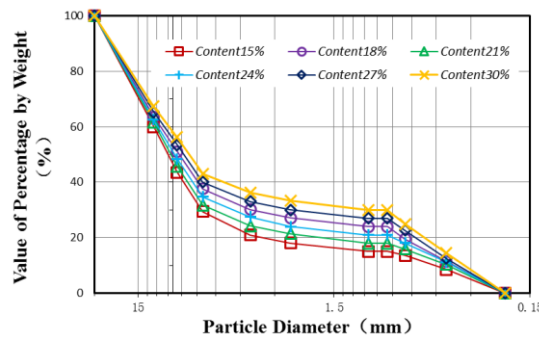


Fig. 7 Grain-size distribution curves of some samples

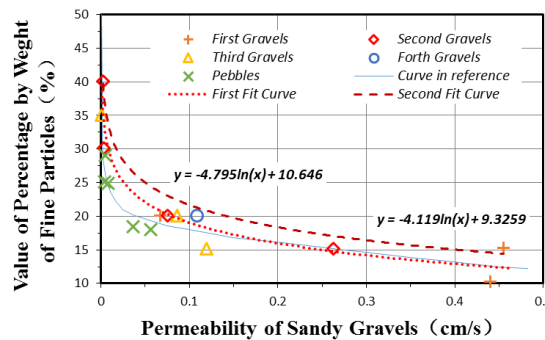


Fig. 8 Experimental results and fit curves between fine particles content and sandy gravels permeability

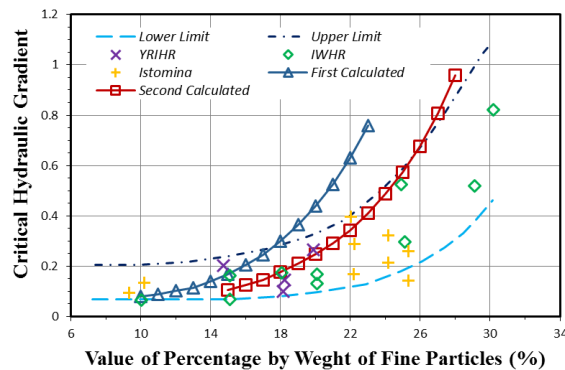


Fig. 9 Curves between fine particles content and critical hydraulic gradient for seepage failure

The relationship between fine particles content and sandy gravels permeability has been obtained through experiments as shown in Fig. 8 (Liu 1963). Four types of gravels and one type of pebbles are analysed in previous experiments. A fit curve (first fit curve) between content and permeability is proposed innovatively according to the four sandy gravels, and the expression of the first fit curve is given, as shown in Fig. 8. There is a permeability upper limit corresponding to each content value. Thus, another fit curve (second fit curve) is proposed according to permeability upper limit, and expression of the second fit curve is also given, as shown in Fig. 8.

Critical hydraulic gradients for seepage failure of samples are calculated by the innovative method. All fit curves are applied in calculations. Results are given respectively and compared with previous research achievements (Liu 1963, Liu 1992). Curves between fine particles content and critical hydraulic gradient for seepage failure are shown in Fig. 9.

Results based on the second fit curve are more consistent with previous experiment achievements according to these curves. The critical hydraulic gradient increases with the fine particles content. In addition, the critical hydraulic gradient is smaller in lower-permeability soil. Although there are some differences between calculated results and previous experiment achievements, the alternation tendency of critical hydraulic gradient is accordant.

5.3 Discussion

Permeability of hypothetical soil is an important coefficient for calculating curvature and quantity of capillary. However, theory methods are not mature. In addition, it is difficult to measure it by experiments. Thus, the problem of defining the permeability needs to be studied.

Drag force and uplift force control fine particles migration. Researches about calculating drag force coefficient are relatively sufficient. Yet determining methods for uplift force coefficient are rare. Previous researches have proved that values of drag force and uplift force belong to the same order of magnitude. C_L is equal to a quarter of C_D based on previous achievements. The accurate determining methods for uplift force need to be researched through many experiments.

Particle C is subject to friction and normal force from the front particle, as shown in Fig. 3. So, particle C will rotate around contact point under the action of drag force, uplift force and effective gravity. In addition, particle C no longer touches the back particle. Actually, this is a simplified condition because the back particle will contribute a resistance when particle C attempts to rotate. However, the resistance is hard to define.

6. Conclusions

- An innovative spiral variable-section capillary model for piping critical hydraulic gradient in cohesion-less soils causing water/mud inrush in tunnels is proposed. The proposed capillary model established relationships between curvature and grain-size distribution, porosity, permeability. Curvature is put forward to describe the actual winding seepage channel of soil. In addition, piping-typed soil particles are classified into coarse particles and fine particles according to grain-size distribution. Pore space of hypothetical soil is simplified to a series of spiral variable-section capillaries.

- The piping critical hydraulic gradient is obtained by analysing starting modes of fine particles and solving corresponding moment equilibrium equations. Gravity, drag force and uplift force are analysed in moment equilibrium equations. In addition, the influence of drag force and uplift force on incipient motion is generally expounded based on the mechanical analysis. Incipient velocities for particles in different arrangements are different.

- Two cases are studied with this capillary model. Critical hydraulic gradients of different sandy gravels with a bimodal grain-size-distribution is obtained in case one. Results have a good agreement with experimental observations by A.W. Skempton and J.M. Brogan. Relationships between content of fine particles and critical hydraulic gradient for seepage failure are analysed in case two. The alternation tendency of critical hydraulic gradient is accordant with experiments.

Acknowledgments

The authors appreciate the support from the National Natural Science Foundation of China (Grant No.: 51509147, 51479106), the National Basic Research Program of China (973 Program, No.: 2013CB036000), and the promotive research fund for excellent young and middle-aged scientists of Shandong Province (Grant No.: BS2014NJ004).

References

- Aberg, B. (1992), "Void ratio of noncohesive soils and similar materials", *J. Geotech. Eng.*, **118**(9), 1315-1334.
- Bai, H.B., Ma, D. and Chen, Z.Q. (2013), "Mechanical behavior of groundwater seepage in karst collapse pillars", *Eng. Geol.*, **164**, 101-106.
- Chang, D.S. and Zhang, L.M. (2013), "Critical hydraulic gradients of internal erosion under complex stress states", *J. Geotech. Geoenviron. Eng.*, **139**(9), 1454-1467.
- Chen, J., Wang, S., Liang, Y., Wang, Y. and Luo, Y. (2015), "Experimental investigation of the erosion mechanisms of piping", *Soil Mech. Found. Eng.*, **52**(5), 301-309.
- Chen, S.S., Zhong, Q.M. and Cao, W.B. (2012), "Breach mechanism and numerical simulation for seepage failure of earth-rock dams", *Sci. Chin. Technol. Sci.*, **55**(6), 1757-1764.
- Han, Q.W. and He, M.M. (1999), *Law of Incipient Motion and Incipient Velocity for Sediment*, Science Press.
- Indraratna, B. and Radampola, S. (2002), "Analysis of critical hydraulic gradient for particle movement in filtration", *J. Geotech. Geoenviron. Eng.*, **128**(4), 347-350.
- Kempton, A.W. and Brogan, J.M. (1994), "Experiments on piping in sandy gravels", *Geotech.*, **44**(3), 449-460.

- Li, S.C., Wu, J., Xu, Z.H., Li, L.P., Huang, X., Xue, Y.G. and Wang, Z.C. (2016), "Numerical analysis of water flow characteristics after intruding from the tunnel floor in process of karst tunnel excavation", *Geomech. Eng.*, **10**(4), 471-526.
- Li, Z.R., Chen, Y.E. and Zhao, Z. (1983), "Experimental research on thrust and uplift force act on sphere on bed surface", *Proceedings of the 2nd International Symposium on River Sedimentation*, Nanjing, China, October.
- Liu, J. (1963), "Seepage stability of sandy gravels with a bimodal grain-size-distribution", *Proceedings of the China Institute of Water Resources and Hydropower Research*, Beijing, China.
- Liu, J. (1992), *Seepage Stability and Seepage Control of Soils*, Water Resources and Electric Power Press, Beijing, China.
- Liu, T.Y., Cao, P. and Lin, H. (2013), "Analytical solutions for the seepage induced fracture failure propagation in rock mass", *Dis. Adv.*, **6**(1), 307-314.
- Liu, Z.Y. (2001), "On the mechanism of piping in noncohesive soils", Ph.D. Dissertation, Lanzhou University, Lanzhou, China.
- Liu, Z.Y., Le, J.C. and Miao, T.D. (2004), "Capillary-tube model for piping in noncohesive soils and its application", *Chin. J. Rock Mech. Eng.*, **23**(22), 3871-3876.
- Ma, D., Miao, X.X. and Bai, H.B. (2016), "Effect of mining on shear sidewall groundwater intrush hazard caused by seepage instability of the penetrated karst collapse pillar", *Nat. Haz.*, **82**(1), 73-93.
- Moffat, R. and Fannin, R.J. (2011), "A hydromechanical relation governing internal stability of cohesionless soil", *Can. Geotech. J.*, **48**(3), 413-424.
- Ni, X., Wang, Y. and Lu, Y. (2010), "Study of meso-mechanism of seepage failure in tunnel excavation process", *Chin. J. Rock Mech. Eng.*, **29**(S2), 4194-4201.
- Ojha, C.S.P., Singh, V.P. and Adrian, D.D. (2003), "Determination of critical head in soil piping", *J. Hydraul. Eng.*, **129**(7), 511-518.
- Okeke, A.C. and Wang, F. (2016), "Hydromechanical constraints on piping failure of landslide dams: An experimental investigation", *Geoenviron. Dis.*, **3**(1), 4.
- Qin, C.B., Sun, Z.B. and Liang, Q. (2013), "Limit analysis of roof collapse in tunnels under seepage forces condition with three-dimensional failure mechanism", *J. Centr. South U.*, **20**(8), 2314-2322.
- Qin, J.S. and Li, A.F. (2004), *Physical Properties of Petroleum Reservoir*, China University of Petroleum Press.
- Richards, K.S. and Reddy, K.R. (2007), "Critical appraisal of piping phenomena in earth dams", *Bull Eng. Geol. Environ.*, **66**(4), 381-402.
- Serdar, K., Tomas, M., Fernandez, S. and Rafiq, A. (2015), "A numerical study on the seepage failure by heave in sheeted excavation pits", *Geomech. Eng.*, **9**(4), 513-530.
- Stokes, G.G. (1851), "On the effect of the internal friction of fluids on the motion of pendulums", *Cambridge Philo. Soc.*, **9**(2), 8-106.
- Wang, Y., Wang, S. J., Duan, X. B., Gu, Y. C., Pang, Q. and Yang, C. (2015), "Physical modelling of initial seepage failure process", *J. Phys. Model. Geotech.*, **15**(4), 1-9.
- Yang, K.H. and Wang, J.Y. (2016), "Experiment and statistical assessment on piping failures in soils with different gradations", *Mar. Georesour. Geotechnol.*, **35**(4), 512-527.
- Yang, X.L. and Yan, R.M. (2015), "Collapse mechanism for deep tunnel subjected to seepage force in layered soils". *Geomech. Eng.*, **8**(5), 741-756.
- Zakaraya Alhasan, M.H., Julínek, T. and Říha, J. (2015), "Discussion on the critical hydraulic gradient for uniform homogeneous glass beads", *Proceedings of the 16th Dam Monitoring International Conference-TKZ, Wierchomla*, Poland, September.
- Zhou, Z.Q., Li, S.C., Li, L.P., Shi, S.S. and Xu, Z.H. (2015), "An optimal classification method for risk assessment of water intrush in karst tunnels based on grey system theory", *Geomech. Eng.*, **8**(5), 631-647.